Magn Reson Med Sci

REVIEW

E-pub ahead of print by J-STAGE
doi:10.2463/mrms.2015-0048

In Vivo Brain MR Imaging at Subnanoliter Resolution: Contrast and Histology

Takashi Watanabe*, Jens Frahm, and Thomas Michaelis

Biomedizinische NMR Forschungs GmbH am Max-Planck-Institut für biophysikalische Chemie 37070 Göttingen, Germany

(Received April 28, 2015; Accepted June 10, 2015; published online September 4, 2015)

This article provides an overview of *in vivo* magnetic resonance (MR) imaging contrasts obtained for mammalian brain in relation to histological knowledge. Emphasis is paid to the (1) significance of high spatial resolution for the optimization of T_1, T_2, and magnetization transfer contrast, (2) use of exogenous extra- and intracellular contrast agents for validating endogenous contrast sources, and (3) histological structures and biochemical compounds underlying these contrasts and (4) their relevance to neuroradiology. Comparisons between MR imaging at subnanoliter resolution and histological data indicate that (a) myelin sheaths, (b) nerve cells, and (c) the neuropil are most responsible for observed MR imaging contrasts, while (a) diamagnetic macromolecules, (b) intracellular paramagnetic ions, and (c) extracellular free water, respectively, emerge as the dominant factors. Enhanced relaxation rates due to paramagnetic ions, such as iron and manganese, have been observed for oligodendrocytes, astrocytes, microglia, and blood cells in the brain as well as for nerve cells. Taken together, a plethora of observations suggests that the delineation of specific structures in high-resolution MR imaging of mammalian brain and the absence of corresponding contrasts in MR imaging of the human brain do not necessarily indicate differences between species but may be explained by partial volume effects. Second, paramagnetic ions are required in active cells *in vivo* which may reduce the magnetization transfer ratio in the brain through accelerated T_1 recovery. Third, reductions of the magnetization transfer ratio may be more sensitive to a particular pathological condition, such as astrocytosis, microglial activation, inflammation, and demyelination, than changes in relaxation. This is because the simultaneous occurrence of increased paramagnetic ions (i.e., shorter relaxation times) and increased free water (i.e., longer relaxation times) may cancel T_1 or T_2 effects, whereas both processes reduce the magnetization transfer ratio.

Keywords: ***gliosis*, *inflammation*, *iron*, *magnetization transfer*, *manganese***

Introduction

Continuous development in magnetic resonance (MR) technology enables investigation of the structure and function of the human body *in vivo* at increasing spatial and temporal resolutions. A minimum voxel size of 58 nl has been shown feasible for such investigation in humans,[1,2] but a resolution below 1 nl (i.e., 100 µm isotropic) is achievable for rodents because their body size allows use of smaller MR imaging magnets and higher field strengths. Although organ sizes differ, most basic histological structures and their respective biochemical compositions are common in all mammals, from humans to mice.[3] This opens new research perspectives by correlating structural and biochemical insights obtained by *in vivo* MR imaging to knowledge obtained by *ex vivo* histology and vice versa. For example, particular neural structures can only be distinguished at a resolution of 0.2 nl or less,[4] which minimizes contrast-eliminating partial volume effects. On the other hand, the diagnostic specificity of MR imaging contrasts for diverse brain pathologies needs further clarification.[5]

*Corresponding author, Phone: +49-551-201-1731, Fax: +49-551-201-1306, E-mail: twatana@gwdg.de

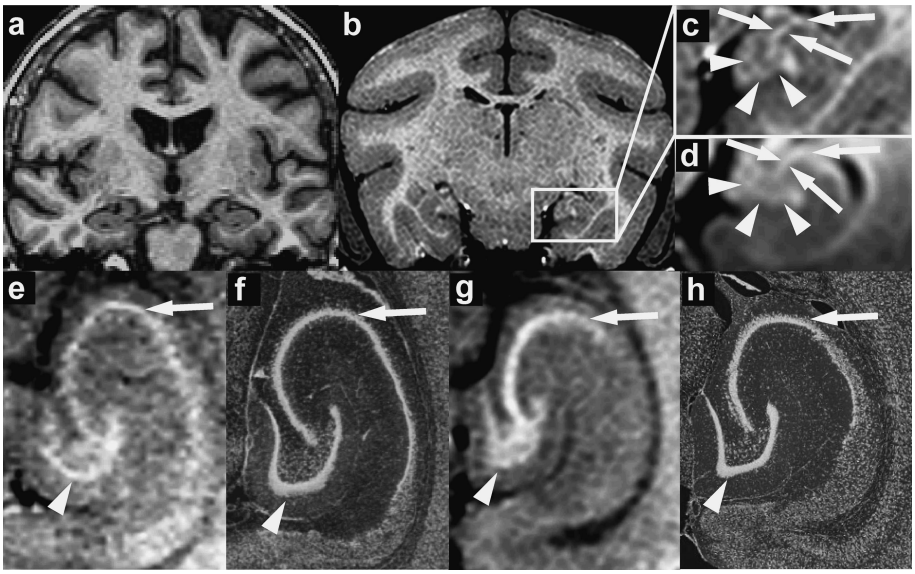

Fig. 1. Endogenous T_1 contrast. Plain T_1-weighted magnetic resonance (MR) imaging of the brain of (**a**) a human and (**b**) a squirrel monkey (voxel size, 27 nl) as well as of the hippocampal formation of (**c**) the squirrel monkey, (**d**) a marmoset (27 nl), and (**e**) a rat (0.9 nl) in comparison with (**f**) a Nissl stain (contrast inverted). (**g**) Plain T_1-weighted MR imaging (0.9 nl) of the hippocampal formation of a mouse in comparison with (**h**) a Nissl stain (contrast inverted). White arrowheads, granule cell layers; white arrows, pyramidal cell layers. See text for details. Adapted with permission.[13–20]

This article provides an overview of current insights into the relation between MR imaging contrast and histological evidence. It emphasizes the (i) significance of subnanoliter resolution for MR imaging to identify the sources of endogenous T_1, T_2, and magnetization transfer (MT) contrast in the brain *in vivo*, (ii) validation of endogenous contrasts via enhancements by the most commonly used exogenous agents, gadolinium chelates and manganese (Mn^{2+}) ions,[6] (iii) histology underlying these basic MR imaging contrasts, and (iv) potential relevance to neuroradiology. We do not consider T_2* contrast induced by exogenous agents because it was recently reviewed elsewhere[7] nor contrasts based on diffusion because subnanoliter resolution was only recently demonstrated *in vivo*.[8]

In vivo Brain MR Imaging

Signal intensities and image contrast in MR imaging of the brain are primarily determined by the spin density of water protons.[2,9,10] However, depending on the technique chosen for data acquisition, a variety of different contrasts may be obtained, which reflect the T_1 or T_2 relaxation properties of mobile water protons, magnetization transfer between water and macromolecular protons, or extra- and intracellular distribution of exogenous contrast agents in brain tissue.

Endogenous T_1 contrast

In general, proton T_1 relaxation processes are strongly promoted if the molecular fluctuation rate and Larmor frequency are on the same order of magnitude.[11] In the human brain, T_1 relaxation of water protons is accelerated by close contact to macromolecular protons, e.g., at myelin sheaths,[12] so that the intensity is higher of white matter (WM) than gray matter (GM) in T_1-weighted (T_1W) MR imaging (Fig. 1a). This WM/GM contrast is preserved through species, e.g., in the squirrel monkey (Fig. 1b). In addition, however, the higher spatial resolution in the latter case also reveals high intensities within the GM, e.g., in the hippocampal formation (arrows and arrowheads, Fig. 1c). This pattern of bright GM signals is preserved from the squirrel monkey to the marmoset (Fig. 1d) and rat (Fig. 1e). Comparison between subnanoliter T_1W MR imaging recordings and histological stains (Fig. 1f) then allows identification of nerve cell assemblies as the source of these bright signals. Extended studies in the mouse brain *in vivo* (Fig. 1g, h) further confirm this endogenous T_1 contrast in the GM.

Endogenous T_2 contrast

Slowly tumbling macromolecules attached to myelin effectively accelerate the T_2 relaxation of nearby water protons in WM.[11] Nevertheless, their

contribution to overall MR imaging contrast is limited because myelin water makes up only a small fraction of WM water[2,21] and because the water exchange between compartments,[12] e.g., between myelin and bulk water, is slow relative to the T_2. As a second mechanism, water proton density may have an even greater influence on WM/GM contrast in T_2-weighted (T_2W) MR imaging because it is affected by the myelin sheaths occupying the extracellular space. In fact, the concomitant reductions in T_2 and proton density caused by myelin contribute to the low signal of WM in T_2W MR imaging, as shown for the human cerebellum *in vivo* (Fig. 2a). Though this pattern of contrast appears to be preserved from humans to the squirrel monkey (Fig. 2b) and marmoset (Fig. 2c), subnanoliter T_2W MR imaging of the cerebellum of a mouse (Fig. 2d) shows additional signal reductions in the GM, i.e., the cortex. This clearly indicates that the myelin sheaths are not the exclusive source of T_2 contrast in the cerebellum *in vivo*. In fact, several studies report a linear relationship between iron content and T_2 in brain tissue.[23–25]

Magnetization transfer

Magnetization transfer techniques[26,27] exploit the cross relaxation between water protons and macromolecular protons, using the conventional MR imaging signal from mobile water protons to detect the effect of broadband excitations of immobilized proton signals that extend over tens of kilohertz and dephase too quickly ($T_2 < 1$ ms) to be visible on MR imaging. The observable decrease of the mobile MR imaging signal is a transferred measure of the saturation of immobilized protons by off-resonance irradiation, which occurs as a combination of dipole-dipole interactions, proton exchange, and water exchange between both pools. The rate of the magnetization transfer is strongly dependent on the relative concentrations of water and macromolecules.[9] Spoiled gradient-echo MR imaging is the method of choice in obtaining magnetization transfer contrast at subnanoliter resolution.[28] Proper off-resonance pulses, moderate echo times, and low flip angles allow for optimized magnetization transfer contrast, while a short repetition time (TR) ensures access to high spatial resolution within a reasonable measuring time.

Figure 2e and f show magnetization transfer contrasts in the cerebella of a marmoset (2e) and mouse (2f) *in vivo*. The magnetization transfer contrast is similar to T_2 contrast, although the areas with MT-reduced intensities are clearly smaller. This confirms that the mechanism underlying MT contrast is different from that of T_2. Strong magnetization transfer occurs in WM (black arrows in Fig. 2e, f) between diamagnetic macromolecules and water, whereas cell assemblies in the cortex have higher concentrations of water and paramagnetic ions than WM. The hydrophilic paramagnetic ions reduce the magnetization transfer effect because the MT saturation of water protons through diamagnetic macromolecules in nerve cells is effectively offset by enhanced T_1 recovery.[28–32]

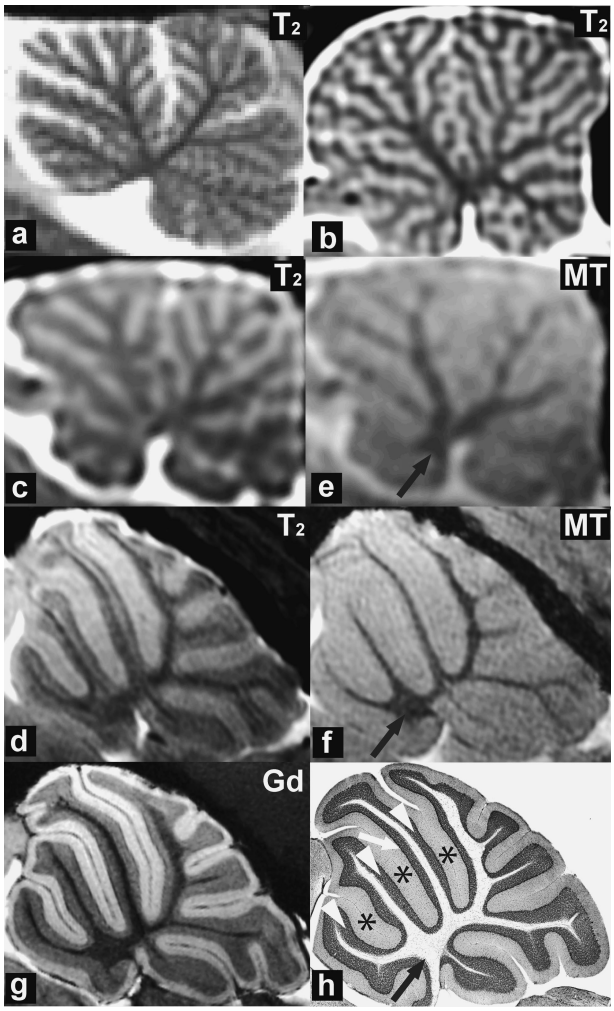

Fig. 2. T_2, magnetization transfer (MT), and gadolinium chelate contrasts. Plain T_2-weighted magnetic resonance (MR) imaging of the cerebellum of (**a**) a human, (**b**) a squirrel monkey (voxel size, 53 nl), (**c**) a marmoset (36 nl), and (**d**) a mouse (0.9 nl) in comparison with plain MT-weighted MR imaging of (**e**) a marmoset (36 nl) and (**f**) a mouse (0.9 nl). (**g**) T_1-weighted MR imaging (voxel size. 0.27 nl) of a mouse after intraventricular injection of gadolinium-diethylenetriamine pentaacetic acid (Gd-DTPA) in comparison with (**h**) a Giemsa stain. Black arrows, white matter; white arrow, Purkinje cell layer; white arrowheads, granule cell layer; asterisks, molecular layer. See text for details. Adapted with permission.[14–16,19,20,22]

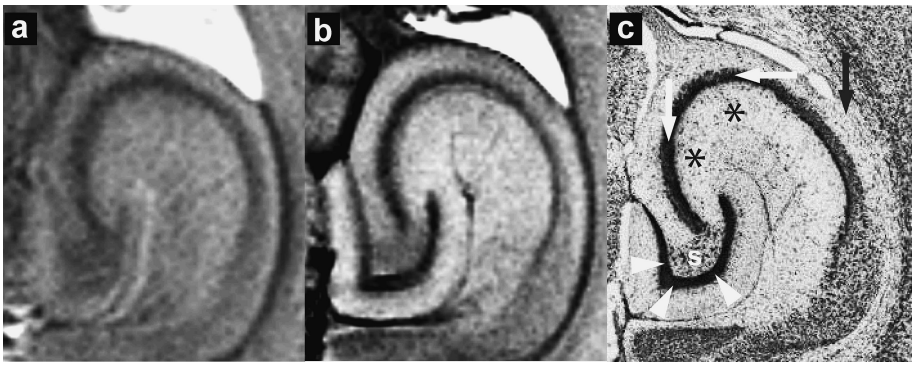

Fig. 3. T_2 and gadolinium chelate contrasts. (**a**) Plain T_2-weighted magnetic resonance (MR) imaging (voxel size, 0.27 nl), (**b**) T_1-weighted MR imaging (voxel size, 0.16 nl) after intraventricular injection of gadolinium-diethylenetriamine pentaacetic acid (Gd-DTPA), and (**c**) a Nissl stain of the hippocampal formation of mice in horizontal sections. Black arrow, white matter; white arrows, pyramidal cell layer; white arrowheads, granule cell layer; asterisks, stratum lacunosum-moleculare; s, strata lucidum and multiforme. See text for details. Adapted with permission.[19,20]

Extracellular agents: gadolinium chelates

Gadolinium chelates are widely used in humans to assess impairment of the blood-brain barrier, through which the agents may reach the extracellular fluid of the brain. Several investigations[33–38] explored the diagnostic potential of their administration into the cerebrospinal fluid in more than 100 human patients. Distributed over the cerebrospinal and extracellular fluid of the entire central nervous system, the chelates induce a unique contrast in brain MR imaging.[19,39–43] In GM, the resulting contrasts are in excellent agreement with histological stains of intracellular compounds.[19] For example, as shown in the cerebellum (Fig. 2g, h), gadolinium chelates generate different signal intensities for the Purkinje cell layer (white arrow), granule cell layer (white arrowheads), and molecular layer (asterisks) in agreement with the histological staining of nerve cells. Similarly, in the hippocampal formation (Fig. 3a-c), plain T_2W MR imaging (Fig. 3a) and gadolinium-enhanced T_1W MR imaging (Fig. 3b) resemble the Nissl-stained histology (Fig. 3c). Neuropil areas (asterisks; the stratum lacunosum-moleculare) show high signal intensity in agreement with their sparse staining, whereas the most densely packed granule cell layer (white arrowheads) and pyramidal cell layer (white arrows) show the lowest signal intensity in agreement with their dense staining. Tissues with moderate staining present with correspondingly low MR imaging signal intensities, e.g., the strata lucidum and multiforme (s in figure). A difference from histology is seen only for WM (black arrows) that presents with the lowest signal intensity in areas that remain unstained.

These findings suggest that the underlying contrast mechanism mainly reflects the ratio of water protons between the intra- and extracellular spaces. In membrane-rich WM, the chelates will be less concentrated because the polar heads of cell membrane lipids hinder the diffusion of the hydrophilic chelates into the hydrophobic region.[28] The same mechanism has been used to improve MR imaging detection of amyloid plaques in the mouse brain[44] because the chelates will be less concentrated in hydrophobic amyloid deposits than the surrounding intact GM. The resulting difference in T_1 between different tissue elements provides T_1W MR imaging with a 16- to 30-fold higher contrast-to-noise ratio[19] compared to that of plain T_2W MR imaging. These observations may help improve understanding of the mechanisms and structures that determine endogenous T_1 and T_2 MR imaging contrast. For example, the similarities between gadolinium-enhanced MR imaging and T_2W MR imaging support the view that the endogenous contrast mainly reflects the extracellular fluid content in tissue.

Intracellular agents: Mn^{2+} ions

Delivery of manganese (Mn^{2+}) ions to the brain can improve contrasts in T_1W MR imaging.[6,7,45] After entering the systemic blood circulation and crossing the capillary endothelium, Mn^{2+} ions are supposed to accumulate in the cytosol,[46] mitochondria,[46,47] lysosomes,[48] and microsomes[49] of brain cells, where they may bind to cytosolic proteins[47,49,50] and inner mitochondrial membranes.[51] The resulting immobilization of Mn^{2+} ions increases their longitudinal relaxivity *in vivo* by reducing the contribution of the rotational correlation time.[32]

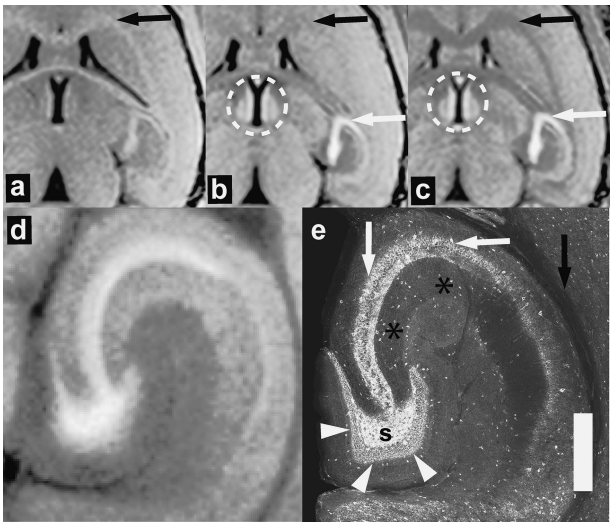

Fig. 4. T_1 contrast and manganese. T_1-weighted magnetic resonance (MR) imaging (voxel size, 1.6 nl) of the brain of a mouse (**a**) before and (**b**) after systemic administration of manganese without and (**c**) with magnetization transfer. (**d**) T_1-weighted MR imaging (voxel size, 0.16 nl) of the hippocampal formation of a mouse after systemic administration of manganese in comparison with (**e**) glutamic acid decarboxylase stain of cell bodies and mossy fibers. Black arrows, white matter; white arrows, pyramidal cell layers; dashed circles, habenular nuclei; white arrowheads, granule cell layer; asterisks, stratum lacunosum-moleculare; s, strata lucidum and multiforme, scale bar = 400 µm. See text for details. Adapted with permission.[19,31,52]

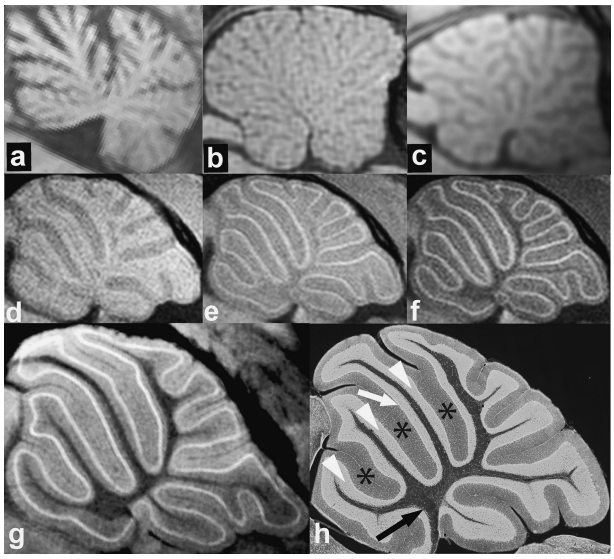

Fig. 5. T_1 contrast and manganese. T_1-weighted magnetic resonance (MR) imaging of the cerebellum of (**a**) a human, (**b**) a squirrel monkey (voxel size, 27 nl), (**c**) a marmoset (27 nl), and (**d**) a mouse (0.64 nl) before and (**e**) after systemic administration of manganese without and (**f**) with magnetization transfer. (**g**) Manganese contrast (voxel size, 0.27 nl) in comparison with (**h**) Giemsa stain (contrast inverted). Black arrow, white matter; white arrow, Purkinje cell layer; white arrowheads, granule cell layer; asterisks, molecular layer. See text for details. Adapted with permission.[13–16,19,20,31]

On the other hand, the ions do not enter the hydrophobic hydrocarbon regions of membranes and will be less concentrated in membrane-rich WM.[30] As a result, Mn^{2+} reverses the contrast between WM (black arrows, Fig. 4) and GM while highlighting the nerve cell assemblies, e.g., in the hippocampal formation and habenula (white arrow and dashed circle), as shown in Fig. 4a and b. Suppression of the WM signal (black arrows, Fig. 4) by MT further improves the contrast induced by Mn^{2+}, as shown in Fig. 4c, because the presence of intracellular paramagnetic ions effectively cancels the magnetization transfer effect in the GM, i.e., on nerve cells.[30–32] At a resolution of 0.16 nl (Fig. 4d), MR imaging reveals that Mn^{2+} also strongly enhances specialized neuropils, i.e., the strata multiforme and lucidum (s in Fig. 4e) despite their smaller intracellular volume (Fig. 3b, c).

Figure 5a-d show almost no endogenous T_1 contrast in the cerebellum of humans and the squirrel monkey, marmoset, and mouse. Only the outermost molecular layer can be distinguished as a rim of low intensity at subnanoliter resolution (Fig. 5d). This observation is in agreement with the view that nerve cells as well as myelin shorten T_1 and T_2 relaxation times (Compare Figs. 1 and 2). Accordingly, as Fig. 5e–h show, the outermost layer of the areas of high intensity is enhanced by Mn^{2+} (the Purkinje cell layer, white arrow). Magnetization transfer saturation further improves the Mn^{2+}-induced contrast by suppressing signals from the neighboring myelinated tissue (black arrow in Fig. 5) while leaving nerve cells unaffected.[30–32]

These MR imaging findings confirm that (1) nerve cells appear bright in plain T_1W MR imaging, (2) Mn^{2+} ions accumulate predominantly in intracellular spaces because their accumulation at outer cell surfaces would enhance the WM more than the cell assemblies and additional MT would reduce the Mn^{2+}-induced contrast, and (3) intracellular paramagnetic ions may counterbalance MT saturation.[30–32] In addition, at high spatial resolution, a comparison of MR imaging contrasts due to Mn^{2+} (Figs. 4d, 5g) and gadolinium chelates (Figs. 2g, 3b) with cell staining (Figs. 1h, 3c, 5h) unravels a discrepancy between Mn^{2+} enhancement and intracellular volume that indicates that Mn^{2+} reflects cellular activity that is disproportionate to

Table 1. Alterations of proton density (PD), relaxation times (T_1, T_2), magnetization transfer ratio (MTR), and concentration of Gd^{3+}-chelates (Gd) or Mn^{2+} ions (Mn) in brain tissues *in vivo*

Tissue	Main chemical component	Examples	PD	T_1	T_2	MTR	Gd	Mn
Myelin	Diamagnetic lipids	White matter	↓↓	↓↓	↓	↑↑	↓	→
Nerve cells	Paramagnetic iron	Globus pallidus, substantia nigra	↓	↓	↓↓	→		↑
	Paramagnetic ions	Pyramidal (HF) and Purkinje (Ce) cell layers		↓↓	↓			
Neuropil	Free water	Stratum lacunosum-moleculare (HF), molecular layer (Ce)	Reference					
Oligodendrocytes	Paramagnetic iron	Stria of Gennari			↓			

Ce, cerebellum; HF, hippocampal formation; decrease (↓) and increase (↑) relative to neuropil

the intracellular space.[19] Most notably, granule cells (white arrowheads in Figs. 4e, 5h) are no more enhanced (Figs. 4d, 5g) than neuropil areas (black asterisks in Figs. 4e, 5h) despite their larger intracellular space (white arrowheads in Figs. 2h, 3c).

Histology

Even the simplest macroscopic inspection readily reveals some regions of freshly cut brain to be shiny white and others that appear darker–the WM and GM. The lipid-rich *myelin* sheaths create the typical appearance of the WM, and the water-rich GM forms a more grayish background. Within the GM, the *nerve cell* bodies, often densely assembled, are surrounded or flanked by the *neuropil*, i.e., feltwork of dendrites and initial/terminal segments of axons.[3] Within particular cerebral cortices, iron ions are most concentrated in a layer in which *oligodendrocytes* actively produce myelin sheaths. Table 1 summarizes the effects of these structural elements and their representative chemical compounds on MR imaging contrasts, and the following sections provide more detailed explanations.

Myelin

Myelin sheaths in the brain represent the extended plasma membranes of oligodendrocytes, which serve as electrical insulators for axonal conduction. Their content of macromolecules (>42%) is higher than that of all other brain tissues (about 6%), and their water content (about 40%) is lower than that of other brain tissues (about 80%).[53–56] Accordingly, WM has less extracellular space[28] and correspondingly less water content (about 70%) than GM (about 80%). This difference in extracellular free water is the prime cause for WM/GM contrast seen by *in vivo* MR imaging. In other words, occupation of the space by the myelin sheaths reduces extracellular fluid content and, thus, water proton density. Without myelin, the WM/GM contrast in T_1W, T_2W, and magnetization transfer MR imaging would be substantially reduced because the water content of the non-myelin portion of brain WM is not different from that of GM (both about 80%).[2,9,10,53,57]

In plain T_2W MR imaging, additional T_2 shortening by myelin may contribute to the WM/GM contrast, although to a limited degree.[2] Whereas immobilized myelin macromolecules accelerate the transverse relaxation of affected water protons (T_2 < 15 ms), the myelin water comprises only a small volume fraction (<15%) in WM,[2,21] and its exchange with other compartments is slow.[12] Accordingly, WM/GM contrast is not much observed in T_2 maps of the human brain[2] because the T_2 is similar of the non-myelin water in WM and the water in GM.[2,21]

With regard to macromolecules, only lipids play a significant role in WM/GM MR imaging contrast because there is no substantial difference in WM/GM concentration in proteins, carbohydrates, or nucleotides.[55] Among brain lipids, galactocerebrosides have a significantly stronger effect than cholesterols or phospholipids on T_1 relaxivity and MT saturation.[58] In plain T_1W MR imaging, WM/GM differences in proton density and relaxation offset each other. At higher magnetic fields, WM/GM contrast is even more difficult to obtain because T_1 relaxation becomes increasingly ineffective.[57] However, the distribution of T_1-shortening gadolinium chelates in extracellular water yields a strong WM/GM T_1 contrast[19] because the contributions of spin density and relaxation again turn additive.

In plain magnetization transfer-weighted MR

imaging, differences in proton density and MT both contribute to the WM/GM contrast. At higher magnetic fields, contrast improves because slower T_1 recovery enhances the MT saturation. The use of exogenous agents can further strengthen the MT contrast for WM/GM[28,30] because (1) polar heads of the lipids prevent the hydrophilic agents from diffusing into the hydrophobic parts of the myelin, (2) the T_1-shortening agents are thus more concentrated in GM than WM, and (3) faster T_1 recovery abolishes the MT saturation of GM water protons.

Nerve cells

In vivo brain MR imaging at subnanoliter resolution (Figs. 1–5) identifies multiple aspects of the cerebral cytoarchitecture that are otherwise difficult to detect.[2] In GM, nerve cell bodies are often tightly assembled as layers or nuclei that play specific roles as functional units. Based on the shorter relaxation times of water in intracellular spaces compared to free water,[59] cell assemblies can be delineated by T_1W,[17,29] T_2W,[19,60] T_2*-weighted,[61] and MT-weighted MR imaging.[29] Comparisons of T_1, T_2, and MT contrast at sufficient resolution indicate that the relaxation enhancement predominantly reflects the presence of paramagnetic ions and does not primarily result from interactions with diamagnetic macromolecules. In comparison with WM, cell assemblies have lower concentrations of diamagnetic macromolecules and greater concentrations of paramagnetic ions, which together contribute to significantly less magnetization transfer and thus enable their distinction from WM.[29] Trace elements in the body and brain, such as iron, zinc, manganese, copper, and selenium ions, which are essential for diverse cellular functions, are more concentrated in GM cell assemblies than WM.[62] Accordingly, administration of Mn^{2+} ions reduces both T_1 and MT significantly more in GM cell assemblies than in WM *in vivo*.[30]

Iron is the most abundant paramagnetic ion in the body and brain. Active cells require iron as a key component of enzymes involved in oxygen transport and metabolism.[63] Most iron is chelated and stored in the protein ferritin as Fe^{3+},[23,63] which shortens water proton T_1 and T_2 relaxation times.[23,64] Accordingly, several studies reported T_1 and T_2 effects as a function of iron content[10,23–25,65] in the human brain, with concentration in the globus pallidus (GP) among the highest. Though T_2W MR imaging shows a similar pattern of signal reduction around the GP (white arrows in Fig. 6a–c) in humans and the squirrel monkey and marmoset, subnanoliter MR imaging of the mouse brain reveals WM structures (black arrows in Fig. 6d) as the internal capsule at the border of the GP (upper white arrows in Fig. 6d). In fact, comparisons with magnetization transfer MR imaging (Fig. 6e, f), which exclusively depicts WM (black arrows in Fig. 6e, f), indicate that low resolution T_2W MR imaging (Fig. 6a–c) alone barely delineates the GP from neighboring WM. For the same reason, the signals of the hippocampal pyramidal cell layers (lower white arrows in Fig. 6d) as well as of the cerebellar Purkinje cell layers (Fig. 2d) are not clearly suppressed by MT (Figs. 2f, 6f) but are reduced in T_2W MR imaging (Figs. 2d, 6d).

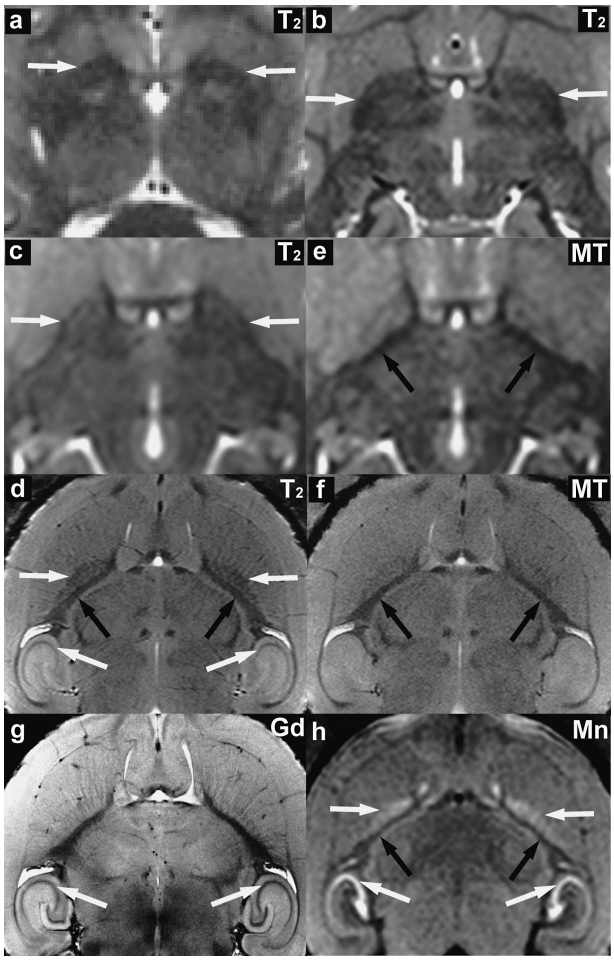

Fig. 6. Endogenous iron contrast. Plain T_2-weighted magnetic resonance (MR) imaging of the brain of (**a**) a human, (**b**) a squirrel monkey (voxel size, 53 nl), (**c**) a marmoset (36 nl), and (**d**) a mouse (0.9 nl) in comparison with plain magnetization transfer-weighted MR imaging of (**e**) a marmoset (36 nl) and (**f**) a mouse (0.9 nl). (**g**) T_1-weighted MR imaging of a mouse after injection of gadolinium-diethylenetriamine pentaacetic acid (Gd-DTPA) into a cerebral ventricle (voxel size, 0.16 nl) and (**h**) manganese into the systemic circulation (voxel size, 1.6 nl). Black arrows, white matter; upper white arrows, globus pallidus; lower white arrows, pyramidal cell layers. See text for details. Adapted with permission.[13–16,19,28,32]

Further, by showing no globus pallidus contrast (Fig. 6g), the administration of gadolinium chelates reveals that the cell packing in the nerve cell assemblies is not particularly tight, so the signal reduction in T_2W MR imaging must result from highly concentrated paramagnetic substances, e.g., iron. Accordingly, Mn^{2+} ions highlight the GP (white arrows in Fig. 6h) in agreement with the observation that the uptake, transport, and storage of Mn^{2+} ions by nerve cells are associated with those of iron and that both iron and manganese concentrations in the GP are the highest in the brain.[66] The GP is most clearly contrasted from neighboring WM (black arrows in Fig. 6h) where myelin hinders the diffusion of Mn^{2+} ions. In contrast, the depiction of the hippocampal pyramidal cell layers–after gadolinium chelate administration (white arrows in Fig. 6g) as well as in T_2W MR imaging (lower white arrows in Fig. 6d)–indicates that both effects result from tight cell packing rather than a high iron concentration in respective cells.

The use of Mn^{2+} ions permits delineation of some highly specialized nerve cells, including the olfactory mitral cells, hippocampal pyramidal cells (white arrows in Fig. 4, lower white arrows in Fig. 6h), and cerebellar Purkinje cells (white arrow in Fig. 5),[19] from the granule cells (white arrowheads in Figs. 4 and 5), although both types of cells are tightly packed (Figs. 2h, 3c) and thus equally enhanced by gadolinium chelates (Figs. 2g, 3b). These findings suggest significant activity of the specialized cells and limited activity of the granule cells to take up Mn^{2+} ions. Mn^{2+} ions also reduce the signals of nerve cells in T_2W MR imaging,[19] which suggests that signal alteration of certain nerve cell assemblies in T_2W MR imaging cannot be ascribed exclusively to iron.

Neuropil

The neuropil areas, composed of interlacing dendrites and axonal terminal ramifications, contain large extracellular and small intracellular spaces. Because of the abundant free water, neuropil areas are characterized by long T_1 and T_2 relaxation times, reduced magnetization transfer, strong enhancement by gadolinium chelates, and weak enhancement by Mn^{2+} ions.[19] As an exception and despite their small intracellular spaces (Fig. 3b, c), a few neuropil areas (e.g., s in Fig. 4e) are even more enhanced by Mn^{2+} ions (Fig. 4d) than granule cell layers (white arrowheads in Fig. 4e) and no less than principal cell layers (white arrows in Fig. 4e). The most likely explanation is their receipt of dense synaptic inputs. For example, the olfactory glomeruli are strongly enhanced,[4,19] while disruption of their synaptic inputs results in significantly reduced enhancement.[67]

Oligodendrocytes

Iron, ferritin, and other paramagnetic ions are required for specific cellular activities and therefore more concentrated in nerve cell assemblies than in myelinated tissue.[23,62] However, in specific neocortices where nerve cells are neither particularly iron-rich nor tightly assembled, iron is most concentrated in layer IV,[2,68] i.e., the outer stripe of Baillarger or the internal granular layer.[69] This is probably attributable to active myelination rather than associated with the granule cells because many lipid-synthesizing enzymes in oligodendrocytes utilize iron as part of their catalytic center.[70] Proteins involved in iron management, i.e., ferritin and transferrin, are also expressed in abundance within oligodendrocytes.[63,70] Accordingly, layer IV in the human visual cortex, well known as the stria of Gennari for its pronounced myelination, can be clearly delineated by MR imaging[1,2] based on a locally increased T_2 relaxation rate. The effect is supposed to be caused by iron rather than macromolecules because the corresponding *ex vivo* MR imaging contrast[68,71] is better co-localized with the iron distribution than with myelin or cell assemblies and is reduced after chemical extraction of tissue iron.[68]

Pathology

The most enlightening insight gained by subnanoliter MR imaging of the rodent brain *in vivo* is the clear identification of myelin- and cell-rich tissues by magnetization transfer saturation as well as their high signal intensities in T_1W MR imaging and correspondingly low signal intensities in T_2W MR imaging. In more detail, diamagnetic macromolecules and intracellular paramagnetic ions both shorten the relaxation times, but differentially increase and decrease[30,31] the MT ratio (MTR), respectively (Table 1). This principle seems valid in pathological conditions as well. Whereas most cells require paramagnetic ions for their proper functioning, pathological accumulations of paramagnetic ions are usually accompanied by a pathological collection of free water, i.e., edema. As a consequence, variable contents of diamagnetic macromolecules, intracellular paramagnetic ions, and free water may lead to complicated biochemical characteristics and diverse alterations of relaxation times and MTR. If, however, the common accumulation of paramagnetic ions and free water and their combined though reverse action on relaxation times

cause no change, then MTR may be a useful measure because both components reduce MTR.

Astrocytes

Despite being the most abundant glial cells in the brain, astrocytes do not strongly contribute to brain MR imaging contrast except in the case of tissue damage that involves astrocytosis. Under oxidative stress, astrocytes may become rich in iron through an overexpression of heme oxygenase-1, an enzyme that promotes mitochondria iron sequestration.[72–74] Thus, the activated iron-rich astrocytes may survive an inflammation and become detectable by MR imaging.[72,75] Furthermore, the manganese-dependent enzymes glutamine synthetase and manganese superoxide dismutase (MnSOD) may be abundant in activated astrocytes. The glutamine synthetase[76–78] is a glia-specific enzymatic protein (astrocytes and oligodendrocytes) that contains 8 Mn^{2+} ions and accounts for approximately 80% of total manganese in the brain. MnSOD is one of the most important antioxidant enzymes[79–82] that protect neurons and glial cells from free radicals. This protein is located in the mitochondria and allows an adaptation of the oxidative metabolism.[83] Its expression is highly regulated by various cytokines,[84,85] e.g., in response to oxidant injury.[82]

Accordingly, focal ischemia induces delayed hyperintensity on T_1W MR imaging of the human brain,[86–89] in agreement with intense MnSOD immunoreactivities[83] in reactive astrocytosis.[86,88] In rats, temporal occlusion of the middle cerebral artery induces delayed hyperintensity on fat-suppressed T_1W (and delayed hypointensity on T_2W) MR imaging in the striatum,[75,87] where the manganese concentration increases in proportion to the induced glutamine synthetase and MnSOD in reactive astrocytes.[75,83,87] The lack of fat signals in localized MR spectra of the rat brain[75] rules out microglial fat[90] as a source of MR imaging contrast. A significantly reduced magnetization transfer ratio[30] would further confirm the presence of iron and/or manganese ions as the dominant source of contrast.

Microglia

Similarly to astrocytes, microglial cells, as the resident macrophages of the central nervous system, do not contribute to MR imaging contrasts unless involved in tissue damage. The smallest glial cells in the brain, microglia react most quickly to scavenge toxic agents and maintain homeostasis. Accordingly, these cells may take up paramagnetic ions that eventually are released from damaged myelin, nerve cells, oligodendrocytes, astrocytes, and blood cells. Microglial cells are able to transform toxic Fe^{2+} ions into more stable Fe^{3+} ions by binding them to ferritin.[71] The resulting accumulation of activated microglias may therefore shorten the T_1 and T_2 relaxation times[64] of affected brain tissue. Microglial cells may also express a high oxygen superoxide scavenging potential related to the presence of MnSOD.[80] Optic nerves of animals with experimental encephalomyelitis showed a 13-fold increase in MnSOD in microglial and phagocytic cells as well as an 8-fold increase in MnSOD in astrocytes in comparison with controls.[91]

Reduced T_2* in *ex vivo* brain MR imaging of a patient with multiple sclerosis co-localized with both oligodendrocytes and activated microglial cells that had taken up iron released by tissue damage.[71] Accordingly, subtle MTR reductions in otherwise normal-appearing WM are associated with marked microglial activation in the brain of patients with multiple sclerosis[92] because intracellular paramagnetic ions are known to reduce MT saturation *in vivo*.[30,32] One MR imaging study[90] using rats observed an accumulation of activated microglia after transient ischemia as a source of T_1 contrast *in vivo* in line with a case report in humans.[88] Given that neither a microglial paramagnetic ion nor potentially concurrent astrocytic manganese accumulation[87] was ruled out, fat-suppressed MR imaging is desirable for investigating lipids[90] as a potential source of contrast.

Hemorrhage

Histological and biochemical underpinnings of the MR imaging contrasts resulting from intracerebral hemorrhage have been described in great detail.[11,93–97] In brief, fresh bleeding consists of free water and intact blood cells for approximately the first 12 hours. In MR imaging, T_1 and T_2 relaxation times of a lesion are longer than or equal to those of normal brain tissue, whereas the magnetization transfer ratio is less than or equal to that of the brain. Subsequently, gradual deoxygenation of oxyhemoglobin in red blood cells mainly shortens T_2 and T_2* at about 12 to 72 hours, and a mild shortening of T_1 in parallel may reduce the MTR. At about 3 to 5 days, a breakdown of blood cells relieves the shortening of T_2 and T_2*. On the other hand, the concurrent conversion from hemoglobin to methemoglobin allows much better access of water to the heme iron, which predominantly shortens T_1 and may also reduce the MTR. Finally, the iron is supposed to be sequestered and crystallized in hemosiderin to minimize its toxic effect, which again shortens T_2. A potential mild reduction of T_1 would reduce the MTR as well.

Table 2. Alterations of relaxation times (T_1, T_2) and magnetization transfer ratio (MTR) in brain pathologies

Component	Pathological involvement	T_1	T_2	MTR
Paramagnetic iron	Ferritin, astrocytes, microglia, macrophages, hemorrhage	↓	↓↓	↓*
Manganese ions	Astrocytes, microglia*	↓↓	↓	↓↓*
Free water	Edema, demyelination	↑↑	↑↑	↓↓

Decrease (↓) and increase (↑) relative to intact tissue; *Estimates based on literature data[11,28,30,64,71,72,87,91,103]

Inflammation

Primary inflammatory changes, which take place in multiple sclerosis as the major demyelinating disorder, share several histopathological characteristics, e.g., perivenous lymphocytic cuffing and myelin sheath swelling,[98] that precede the loss of myelin. Accordingly, lesions are most commonly characterized by locally increased free water content, e.g., edema and demyelination, which typically present with increased proton density, prolonged T_1 and T_2, and reduced MTR. Meanwhile, microglial proliferation[98,99] as well as reactive astrocytosis[100–102] may become prominent in and around the lesion, while iron-rich macrophages[103] and other blood cells[104,105] from the systemic circulation may additionally participate through the impaired blood-brain barrier. In some lesions, partial remyelination may take place. The MR imaging appearance of each of these elements during lesion development may be erratic and difficult to interpret. Several investigations reported poor correlation between visible lesion volume in standard T_2W MR imaging and clinical signs.[106]

Given the fact that intracellular paramagnetic ions and free water may mutually cancel relaxation effects but both reduce MT saturation (Figs. 1, 2, 4, 5, 6),[28–31] there may be a particular inflammatory condition in which the MTR is more sensitive than T_1W or T_2W MR imaging. In other words, longer T_1 and T_2 caused by increased free water content may be counterbalanced by the astrocytic, microglial, macrophagic, or hemorrhagic accumulation of iron and manganese,[71,75,80,87,91] whereas the MTR is reduced by each of these processes (Table 2). For example, an increase in astrocytes and activated microglia appears to outweigh the decrease in oligodendrocytes in plaques,[107] which may offset prolonged relaxation times due to increased free water. In fact, a number of investigations reported a significantly reduced MTR in otherwise normal-appearing WM and GM,[92,106,108–114] a close correlation between the MTR and clinical disability,[114–117] and a potential prognostic value of magnetization transfer MR imaging.[114,118–120] More recent studies suggest that iron-laden/activated microglia[71,121] and/or aggregates typical of small bleeding[71] cause focally increased T_2 relaxation rates and/or reduced MTR[92] within normal-appearing WM. Conflicting results[122] may be explained by heterogeneous and variable patterns in pathology, e.g., the extent of tissue damage and remyelination. For example, apart from astrocytosis or bleeding,[104,105] iron content in a demyelinating lesion may depend on the iron in the remaining tissue as well as on the propensity of microglial cells for accumulating iron released from damaged structures.[71]

Similarly, in encephalitis caused by the human immunodeficiency virus, inflammation leads to the loss of myelin and nerve cells, where reactive astrocytosis and generalized microglial activation take place as prominent pathological features.[123] Recent MR imaging studies found a significant reduction of T_1 and the MTR[124,125] whereas mild T_2* alterations did not correspond to clinical disability. A reduced magnetization transfer ratio may again be explained by T_1 shortening caused by paramagnetic ion accumulation that overrides T_1 lengthening due to increased free water, whereas prolongation of T_2 due to free water may compensate for concurrent T_2 shortening.

Neoplasms

A number of investigations examined the use of T_1, T_2, and MTR for the diagnosis and assessment of brain tumors.[106] In particular, significantly higher MTR values are shown in solid high grade gliomas and collagen-rich meningiomas than low grade gliomas.[126–128] The increased magnetization transfer saturation most likely results from increased diamagnetic macromolecules and reduced free water. On the other hand, an area of WM of reduced magnetization transfer at the periphery of metastatic tumors,[96,129] which appears normal in T_2W MR imaging, suggests a locally increased concentration of paramagnetic ions caused by activated microglia, astrocytes, and/or spreading tumor cells, which shorten T_2 and offset its prolongation caused by edema or demyelination.

Conclusion

Recent investigations at increasingly high spatial resolution unraveled the major sources of MR imaging contrasts in mammalian brain *in vivo* in relation to the underlying histological context. Exogenous T_1 shortening by extra- and intracellular agents contributes to the validation of endogenous contrast sources by improving the contrast-to-noise ratio and/or spatial resolution as well as by facilitating direct comparisons with histological data. Myelin, nerve cells, and neuropil determine the basic *in vivo* MR imaging contrasts by their diamagnetic macromolecules, intracellular paramagnetic ions, and extracellular free water. Given the observation that only high resolution MR imaging delineates specific brain structures, the lack of corresponding contrasts in MR imaging of the human brain does not necessarily represent a histological difference between species but may be ascribed to partial volume effects. In addition, reduced relaxation times are reported for cells associated with disorder, e.g., activated glial cells, which require paramagnetic iron and/or manganese ions for their activities. Accordingly, the magnetization transfer ratio may be reduced by elevated concentrations of paramagnetic ions as well as by increased tissue fluids, whereas these processes may counterbalance potential alterations in relaxation times.

References

1. Duyn JH, van Gelderen P, Li TQ, de Zwart JA, Koretsky AP, Fukunaga M. High-field MRI of brain cortical substructure based on signal phase. Proc Nat Acad Sci USA 2007; 104:11796–11801.
2. Turner R. MRI methods for *in-vivo* cortical parcellation, In: Geyer S, Turner R, eds. Microstructural parcellation of the human cerebral cortex. Berlin Heidelberg: Springer, 2013; 197–220.
3. Nieuwenhuys R, Ten Donkelaar HJ, Nicholson C. The central nervous system of vertebrates. Volume 3. Berlin Heidelberg: Springer, 1998.
4. Chuang KH, Belluscio L, Koretsky AP. *In vivo* detection of individual glomeruli in the rodent olfactory bulb using manganese enhanced MRI. Neuroimage 2010; 49:1350–1356.
5. Filippi M, Dousset V, McFarland HF, Miller DH, Grossman RI. Role of magnetic resonance imaging in the diagnosis and monitoring of multiple sclerosis: consensus report of the White Matter Study Group. J Magn Reson Imaging 2002; 15:499–504.
6. Koretsky AP, Silva AC. Manganese-enhanced magnetic resonance imaging (MEMRI). NMR Biomed 2004; 17:527–531.
7. Duyn JH, Koretsky AP. Novel frontiers in ultrastructural and molecular MRI of the brain. Curr Opin Neurol 2011; 24:386–393.
8. Wu D, Reisinger D, Xu J, et al. Localized diffusion magnetic resonance micro-imaging of the live mouse brain. Neuroimage 2014; 91:12–20.
9. Fralix TA, Ceckler TL, Wolff SD, Simon SA, Balaban RS. Lipid bilayer and water proton magnetization transfer: effect of cholesterol. Magn Reson Med 1991; 18:214–223.
10. Gelman N, Ewing JR, Gorell JM, Spickler EM, Solomon EG. Interregional variation of longitudinal relaxation rates in human brain at 3.0 T: relation to estimated iron and water contents. Magn Reson Med 2001; 45:71–79.
11. Weisskoff RM, Edelman RR. Basic principles of MRI, In: Edelman RR, Hesselink JR, Zlatkin MB, eds. Clinical magnetic resonance imaging, 2nd ed. Philadelphia: WB Saunders Company, 1996; 3–51.
12. Koenig SH, Brown RD 3rd, Spiller M, Lundbom N. Relaxometry of brain: why white matter appears bright in MRI. Magn Reson Med 1990; 14:482–495.
13. Johnson KA, Becker JA. Whole brain atlas. 1995, www.med.harvard.edu/AANLIB/home.html
14. Boretius S, Natt O, Watanabe T, et al. *In vivo* diffusion tensor mapping of the brain of squirrel monkey, rat, and mouse using single-shot STEAM MRI. MAGMA 2004; 17:339–347.
15. Tammer R, Ehrenreich L, Boretius S, Watanabe T, Frahm J, Michaelis T. Compatibility of glass-guided recording microelectrodes in the brain stem of squirrel monkeys with high-resolution 3D MRI. J Neurosci Methods 2006; 153:221–229.
16. Boretius S, Schmelting B, Watanabe T, et al. Monitoring of EAE onset and progression in the common marmoset monkey by sequential high-resolution 3D MRI. NMR Biomed 2006; 19:41–49.
17. Watanabe T, Frahm J, Michaelis T. Functional mapping of neural pathways in rodent brain *in vivo* using manganese-enhanced three-dimensional magnetic resonance imaging. NMR Biomed 2004; 17: 554–568.
18. Paxinos G, Watson C. The rat brain in stereotaxic coordinates. 4th ed. San Diego: Academic Press, 1998.
19. Watanabe T, Frahm J, Michaelis T. Cell layers and neuropil: contrast-enhanced MRI of mouse brain *in vivo*. NMR Biomed 2013; 26:1870–1878.
20. Mikula S, Trotts I, Stone JM, Jones EG. Internet-enabled high-resolution brain mapping and virtual microscopy. Neuroimage 2007; 35:9–15. http://brainmaps.org
21. Whittall KP, MacKay AL, Graeb DA, Nugent RA, Li DK, Paty DW. *In vivo* measurement of T_2 distributions and water contents in normal human brain. Magn Reson Med 1997; 37:34–43.
22. Nalini A, Ramakrishna A, Dekumoy P, et al. Severe form of radiculo-myelo-neuropathy with meningoencephalitis secondary to Angiostrongylus canto-

nensis infection: unusual corpus callosal lesions and serial magnetic resonance imaging findings. Neurol India 2013; 61:414–418.
23. Haacke EM, Cheng NY, House MJ, et al. Imaging iron stores in the brain using magnetic resonance imaging. Magn Reson Imaging 2005; 23:1–25.
24. Langkammer C, Krebs N, Goessler W, et al. Quantitative MR imaging of brain iron: a postmortem validation study. Radiology 2010; 257:455–462.
25. Mitsumori F, Watanabe H, Takaya N. Estimation of brain iron concentration *in vivo* using a linear relationship between regional iron and apparent transverse relaxation rate of the tissue water at 4.7T. Magn Reson Med 2009; 62:1326–1330.
26. Henkelman RM, Stanisz GJ, Graham SJ. Magnetization transfer in MRI: a review. NMR Biomed 2001; 14:57–64.
27. Sled JG, Pike GB. Quantitative imaging of magnetization transfer exchange and relaxation properties *in vivo* using MRI. Magn Reson Med 2001; 46: 923–931.
28. Watanabe T, Frahm J, Michaelis T. Myelin mapping in the central nervous system of living mice using contrast-enhanced magnetization transfer MRI. Neuroimage 2012; 63:812–817.
29. Natt O, Watanabe T, Boretius S, Frahm J, Michaelis T. Magnetization transfer MRI of mouse brain reveals areas of high neural density. Magn Reson Imaging 2003; 21:1113–1120.
30. Watanabe T, Frahm J, Michaelis T. Myelin mapping in the living mouse brain using manganese-enhanced magnetization transfer MRI. Neuroimage 2010; 49:1200–1204.
31. Watanabe T, Frahm J, Michaelis T. Mapping of cellular layers in mouse brain and spinal cord using magnetization transfer and manganese. Proc Int Soc Magn Reson Med 2010:304. http://cds.ismrm.org/protected/10Presentations/304/
32. Watanabe T, Frahm J, Michaelis T. Reduced intracellular mobility underlies manganese relaxivity in mouse brain *in vivo*: MRI at 2.35 and 9.4 T. Brain Struct Funct 2015; 220:1529–1538.
33. Siebner HR, Gräfin von Einsiedel H, Conrad B. Magnetic resonance ventriculography with gadolinium DTPA: report of two cases. Neuroradiology 1997; 39:418–422.
34. Reiche W, Komenda Y, Schick B, Grunwald I, Steudel W, Reith W. MR cisternography after intrathecal Gd-DTPA application. Eur Radiol 2002; 12: 2943–2949.
35. Jinkins JR, Rudwan M, Krumina G, Tali ET. Intrathecal gadolinium-enhanced MR cisternography in the evaluation of clinically suspected cerebrospinal fluid rhinorrhea in humans: early experience. Radiology 2002; 222:555–559.
36. Tali ET, Ercan N, Krumina G, et al. Intrathecal gadolinium (gadopentetate dimeglumine) enhanced magnetic resonance myelography and cisternography: results of a multicenter study. Invest Radiol 2002; 37:152–159.
37. Aydin K, Guven K, Sencer S, Jinkins JR, Minareci O. MRI cisternography with gadolinium-containing contrast medium: its role, advantages and limitations in the investigation of rhinorrhoea. Neuroradiology 2004; 46:75–80.
38. Joseph VB, Raghuram L, Korah IP, Chacko AG. MR ventriculography for the study of CSF flow. AJNR Am J Neuroradiol 2003; 24:373–381.
39. Mavioglu H, Tuglu I, Temiz C, et al. Clinical and histological changes of intrathecally administered gadopentate dimeglumine (Gd-DTPA) in normal rats. Riv Neuroradiol 2005; 18:521–528.
40. Wan XM, Fu TC, Smith PH, Brainard JR, London RE. Magnetic resonance imaging study of the rat cerebral ventricular system utilizing intracerebrally administered contrast agents. Magn Reson Med 1991; 21:97–106.
41. Toney GM, Chavez HA, Ibarra R, Jinkins JR. Acute and subacute physiological and histological studies of the central nervous system after intrathecal gadolinium injection in the anesthetized rat. Invest Radiol 2001; 36:33–40.
42. Liu CH, D'Arceuil HE, de Crespigny AJ. Direct CSF injection of $MnCl_2$ for dynamic manganese-enhanced MRI. Magn Reson Med 2004; 51:978–987.
43. Watanabe T, Tammer R, Boretius S, Frahm J, Michaelis T. Chromium(VI) as a novel MRI contrast agent for cerebral white matter: preliminary results in mouse brain *in vivo*. Magn Reson Med 2006; 56:1–6.
44. Petiet A, Santin M, Bertrand A, et al. Gadolinium-staining reveals amyloid plaques in the brain of Alzheimer's transgenic mice. Neurobiol Aging 2012; 33:1533–1544.
45. Aoki I, Wu YJ, Silva AC, Lynch RM, Koretsky AP. *In vivo* detection of neuroarchitecture in the rodent brain using manganese-enhanced MRI. Neuroimage 2004; 22:1046–1059.
46. Liccione JJ, Maines MD. Selective vulnerability of glutathione metabolism and cellular defense mechanisms in rat striatum to manganese. J Pharmacol Exp Ther 1988; 247:156–161.
47. Wedler FC, Ley BW, Grippo AA. Manganese(II) dynamics and distribution in glial cells cultured from chick cerebral cortex. Neurochem Res 1989; 14:1129–1135.
48. Suzuki H, Wada O, Inoue K, Tosaka H, Ono T. Role of brain lysosomes in the development of manganese toxicity in mice. Toxicol Appl Pharmacol 1983; 71:422–429.
49. Komura J, Sakamoto M. Subcellular and gel chromatographic distribution of manganese in the mouse brain: relation to the chemical form of chronically-ingested manganese. Toxicol Lett 1993; 66: 287–294.
50. Wedler FC, Ley BW. Kinetic, ESR, and trapping evidence for *in vivo* binding of Mn(II) to glutamine

synthetase in brain cells. Neurochem Res 1994; 19: 139–144.
51. Gunter TE, Puskin JS, Russell PR. Quantitative magnetic resonance studies of manganese uptake by mitochondria. Biophys J 1975; 15:319–333.
52. Jinno S, Aika Y, Fukuda T, Kosaka T. Quantitative analysis of GABAergic neurons in the mouse hippocampus, with optical disector using confocal laser scanning microscope. Brain Res 1998; 814:55–70.
53. Norton WT. Myelin: structure and biochemistry, In: Tower DB, ed. The nervous system. Vol. 1: The basic neurosciences. New York: Raven Press, 1975; 467–481.
54. Agranoff BW, Hajra AK. Lipids, In: Siegel GJ, Agranoff BW, Albers RW, Molinoff PB, eds. Basic neurochemistry: molecular, cellular, and medical aspects. 4th ed. New York: Raven Press, 1994; 97–116.
55. Clausen J. Gray-white matter differences, In: Lajtha A, ed. Handbook of neurochemistry. Volume 1. Chemical architecture of the nervous system. New York: Plenum Press, 1969; 273–300.
56. Katzman R, Schimmel H. Water movement, In: Lajtha A, ed. Handbook of Neurochemistry. Volume 2. Structural neurochemistry. New York: Plenum Press, 1969; 11–22.
57. Fischer HW, Van Haverbeke Y, Schmitz-Feuerhake I, Muller RN. The uncommon longitudinal relaxation dispersion of human brain white matter. Magn Reson Med 1989; 9:441–446.
58. Kucharczyk W, Macdonald PM, Stanisz GJ, Henkelman RM. Relaxivity and magnetization transfer of white matter lipids at MR imaging: importance of cerebrosides and pH. Radiology 1994; 192:521–529.
59. Schoeniger JS, Aiken N, Hsu E, Blackband SJ. Relaxation-time and diffusion NMR microscopy of single neurons. J Magn Reson B 1994; 103:261–273.
60. Boretius S, Kasper L, Tammer R, Michaelis T, Frahm J. MRI of cellular layers in mouse brain *in vivo*. Neuroimage 2009; 47:1252–1260.
61. Baltes C, Radzwill N, Bosshard S, Marek D, Rudin M. Micro MRI of the mouse brain using a novel 400 MHz cryogenic quadrature RF probe. NMR Biomed 2009; 22:834–842.
62. Prohaska JR. Functions of trace elements in brain metabolism. Physiol Rev 1987; 67:858–901.
63. Que EL, Domaille DW, Chang CJ. Metals in neurobiology: probing their chemistry and biology with molecular imaging. Chem Rev 2008; 108:1517–1549.
64. Vymazal J, Zak O, Bulte JW, Aisen P, Brooks RA. T_1 and T_2 of ferritin solutions: effect of loading factor. Magn Reson Med 1996; 36:61–65.
65. Drayer B, Burger P, Darwin R, Riederer S, Herfkens R, Johnson GA. MRI of brain iron. AJR Am J Roentgenol 1986; 147:103–110.
66. Aschner M, Guilarte TR, Schneider JS, Zheng W. Manganese: recent advances in understanding its transport and neurotoxicity. Toxicol Appl Pharmacol 2007; 221:131–147.
67. Watanabe T, Schachtner J, Krizan M, Boretius S, Frahm J, Michaelis T. Manganese-enhanced 3D MRI of established and disrupted synaptic activity in the developing insect brain *in vivo*. J Neurosci Methods 2006; 158:50–55.
68. Fukunaga M, Li TQ, van Gelderen P, et al. Layer-specific variation of iron content in cerebral cortex as a source of MRI contrast. Proc Nat Acad Sci USA 2010; 107:3834–3839.
69. Nieuwenhuys R. The myeloarchitectonic studies on the human cerebral cortex of the Vogt-Vogt school, and their significance for the interpretation of functional neuroimaging data, In: Geyer S, Turner R, eds. Microstructural parcellation of the human cerebral cortex. Berlin Heidelberg: Springer, 2013; 55–125.
70. LeVine SM, Chakrabarty A. The role of iron in the pathogenesis of experimental allergic encephalomyelitis and multiple sclerosis. Ann N Y Acad Sci 2004; 1012:252–266.
71. Bagnato F, Hametner S, Yao B, et al. Tracking iron in multiple sclerosis: a combined imaging and histopathological study at 7 Tesla. Brain 2011; 134(Pt 12):3602–3615.
72. Bian W, Harter K, Hammond-Rosenbluth KE, et al. A serial *in vivo* 7T magnetic resonance phase imaging study of white matter lesions in multiple sclerosis. Mult Scler 2013; 19:69–75.
73. Mehindate K, Sahlas DJ, Frankel D, et al. Proinflammatory cytokines promote glial heme oxygenase-1 expression and mitochondrial iron deposition: implications for multiple sclerosis. J Neurochem 2001; 77:1386–1395.
74. Schipper HM. Heme oxygenase-1: transducer of pathological brain iron sequestration under oxidative stress. Ann N Y Acad Sci 2004; 1012:84–93.
75. Wang X, Qian J, He R, et al. Delayed changes in T_1-weighted signal intensity in a rat model of 15-minute transient focal ischemia studied by magnetic resonance imaging/spectroscopy and synchrotron radiation X-ray fluorescence. Magn Reson Med 2006; 56:474–480.
76. Martinez-Hernandez A, Bell KP, Norenberg MD. Glutamine synthetase: glial localization in brain. Science 1977; 195:1356–1358.
77. Wedler FC, Denman RB. Glutamine synthetase: the major Mn (II) enzyme in mammalian brain. Curr Top Cell Regul 1984; 24:153–169.
78. Tansey FA, Farooq M, Cammer W. Glutamine synthetase in oligodendrocytes and astrocytes: new biochemical and immunocytochemical evidence. J Neurochem 1991; 56:266–272.
79. Villafranca JJ, Yost FJ Jr, Fridovich I. Magnetic resonance studies of manganese(3) and iron(3) superoxide dismutases. Temperature and frequency de-

pendence of proton relaxation rates of water. J Biol Chem 1974; 249:3532–3536.
80. Pinteaux E, Perraut M, Tholey G. Distribution of mitochondrial manganese superoxide dismutase among rat glial cells in culture. Glia 1998; 22:408–414.
81. McCord JM, Fridovich I. Superoxide dismutase: an enzymatic function for erythrocuprein (hemocuprein). J Biol Chem 1969; 244:6049–6055.
82. Pinteaux E, Copin JC, Ledig M, Tholey G. Modulation of oxygen-radical-scavenging enzymes by oxidative stress in primary cultures of rat astroglial cells. Dev Neurosci 1996; 18:397–404.
83. Zhang P, Anglade P, Hirsch EC, Javoy-Agid F, Agid Y. Distribution of manganese-dependent superoxide dismutase in the human brain. Neuroscience 1994; 61:317–330.
84. Visner GA, Dougall WC, Wilson JM, Burr IA, Nick HS. Regulation of manganese superoxide dismutase by lipopolysaccharide, interleukin-1, and tumor necrosis factor. Role in the acute inflammatory response. J Biol Chem 1990; 265:2856–2864.
85. Kifle Y, Monnier J, Chesrown SE, Raizada MK, Nick HS. Regulation of the manganese superoxide dismutase and inducible nitric oxide synthase gene in rat neuronal and glial cells. J Neurochem 1996; 66:2128–2135.
86. Ohara S, Nakagawa S, Tabata K, Hashimoto T. Hemiballism with hyperglycemia and striatal T1-MRI hyperintensity: an autopsy report. Mov Disord 2001; 16:521–525.
87. Fujioka M, Taoka T, Matsuo Y, et al. Magnetic resonance imaging shows delayed ischemic striatal neurodegeneration. Ann Neurol 2003; 54:732–747.
88. Shan DE, Pan HC, Ho DM, Teng MM, Chang C. Presence of activated microglia in a high-signal lesion on T_1-weighted MR images: a biopsy sample re-examined. AJNR Am J Neuroradiol 2007; 28: 602.
89. Baheti NN, Cherian A, Wattamwar PR, Kesavadas C, Thomas B. Ischemic hyperintensities on T_1-weighted magnetic resonance imaging of patients with stroke: new insights from susceptibility weighted imaging. Neurol India 2010; 58:90–94.
90. Aoe H, Takeda Y, Kawahara H, Tanaka A, Morita K. Clinical significance of T_1-weighted MR images following transient cerebral ischemia. J Neurol Sci 2006; 241:19–24.
91. Qi X, Guy J, Nick H, Valentine J, Rao N. Increase of manganese superoxide dismutase, but not of Cu/Zn-SOD, in experimental optic neuritis. Invest Ophthalmol Vis Sci 1997; 38:1203–1212.
92. Moll NM, Rietsch AM, Thomas S, et al. Multiple sclerosis normal-appearing white matter: pathology-imaging correlations. Ann Neurol 2011; 70: 764–773.
93. Hayman LA, Taber KH, Ford JJ, Bryan RN. Mechanisms of MR signal alteration by acute intracerebral blood: old concepts and new theories. AJNR Am J Neuroradiol 1991; 12:899–907.
94. Gomori JM, Grossman RI, Asakura T, et al. An *in vitro* study of magnetization transfer and relaxation rates of hematoma. AJNR Am J Neuroradiol 1993; 14:871–880.
95. Mittl RL Jr, Gomori JM, Schnall MD, Holland GA, Grossman RI, Atlas SW. Magnetization transfer effects in MR imaging of *in vivo* intracranial hemorrhage. AJNR Am J Neuroradiol 1993; 14:881–891.
96. Grossman RI, Gomori JM, Ramer KN, Lexa FJ, Schnall MD. Magnetization transfer: theory and clinical applications in neuroradiology. Radiographics 1994; 14:279–290.
97. Anzalone N, Scotti R, Riva R. Neuroradiologic differential diagnosis of cerebral intraparenchymal hemorrhage. Neurol Sci 2004; 25 Suppl 1:S3–S5.
98. Lakhampal SK, Maravilla KR. Multiple sclerosis, In: Stark DD, Bradley WG, eds. Magnetic resonance imaging, 3rd ed. St. Louis: Mosby, 1999; 1379–1402.
99. Lucchinetti CF, Popescu BF, Bunyan RF, et al. Inflammatory cortical demyelination in early multiple sclerosis. N Engl J Med 2011; 365:2188–2197.
100. Holley JE, Gveric D, Newcombe J, Cuzner ML, Gutowski NJ. Astrocyte characterization in the multiple sclerosis glial scar. Neuropathol Appl Neurobiol 2003; 29:434–444.
101. Ayers MM, Hazelwood LJ, Catmull DV, et al. Early glial responses in murine models of multiple sclerosis. Neurochem Int 2004; 45:409–419.
102. Misu T, Fujihara K, Kakita A, et al. Loss of aquaporin 4 in lesions of neuromyelitis optica: distinction from multiple sclerosis. Brain 2007; 130(Pt 5): 1224–1234.
103. Ward RJ, Zucca FA, Duyn JH, Crichton RR, Zecca L. The role of iron in brain ageing and neurodegenerative disorders. Lancet Neurol 2014; 13:1045–1060.
104. Craelius W, Migdal MW, Luessenhop CP, Sugar A, Mihalakis I. Iron deposits surrounding multiple sclerosis plaques. Arch Pathol Lab Med 1982; 106: 397–399.
105. Adams CW. Perivascular iron deposition and other vascular damage in multiple sclerosis. J Neurol Neurosurg Psychiatry 1988; 51:260–265.
106. Ulmer JL, Mathews VP, Hamilton CA, Elster AD. Magnetization transfer imaging of the brain, In: Stark DD, Bradley WG, eds. Magnetic resonance imaging, 3rd ed. St. Louis: Mosby, 1999; 1539–1553.
107. Miller DH, Barkhof F, Frank JA, Parker GJ, Thompson AJ. Measurement of atrophy in multiple sclerosis: pathological basis, methodological aspects and clinical relevance. Brain 2002; 125(Pt 8): 1676–1695.
108. Dousset V, Grossman RI, Ramer KN, et al. Experimental allergic encephalomyelitis and multiple sclerosis: lesion characterization with magnetization transfer imaging. Radiology 1992; 182:483–

491.
109. Filippi M, Campi A, Dousset V, et al. A magnetization transfer imaging study of normal-appearing white matter in multiple sclerosis. Neurology 1995; 45(3 Pt 1):478–482.
110. Filippi M, Rocca MA, Martino G, Horsfield MA, Comi G. Magnetization transfer changes in the normal appearing white matter precede the appearance of enhancing lesions in patients with multiple sclerosis. Ann Neurol 1998; 43:809–814.
111. Loevner LA, Grossman RI, Cohen JA, Lexa FJ, Kessler D, Kolson DL. Microscopic disease in normal-appearing white matter on conventional MR images in patients with multiple sclerosis: assessment with magnetization-transfer measurements. Radiology 1995; 196:511–515.
112. Pike GB, De Stefano N, Narayanan S, et al. Multiple sclerosis: magnetization transfer MR imaging of white matter before lesion appearance on T_2-weighted images. Radiology 2000; 215:824–830.
113. Ge Y. Multiple sclerosis: the role of MR imaging. AJNR Am J Neuroradiol 2006; 27:1165–1176.
114. Bar-Zohar D, Agosta F, Goldstaub D, Filippi M. Magnetic resonance imaging metrics and their correlation with clinical outcomes in multiple sclerosis: a review of the literature and future perspectives. Mult Scler 2008; 14:719–727.
115. Gass A, Barker GJ, Kidd D, et al. Correlation of magnetization transfer ratio with clinical disability in multiple sclerosis. Ann Neurol 1994; 36:62–67.
116. De Stefano N, Battaglini M, Stromillo ML, et al. Brain damage as detected by magnetization transfer imaging is less pronounced in benign than in early relapsing multiple sclerosis. Brain 2006; 129(Pt 8): 2008–2016.
117. Lin X, Tench CR, Morgan PS, Constantinescu CS. Use of combined conventional and quantitative MRI to quantify pathology related to cognitive impairment in multiple sclerosis. J Neurol Neurosurg Psychiatry 2008; 79:437–441.
118. Santos AC, Narayanan S, de Stefano N, et al. Magnetization transfer can predict clinical evolution in patients with multiple sclerosis. J Neurol 2002; 249:662–668.
119. Rovaris M, Agosta F, Sormani MP, et al. Conventional and magnetization transfer MRI predictors of clinical multiple sclerosis evolution: a medium-term follow-up study. Brain 2003; 126(Pt 10): 2323–2332.
120. Agosta F, Rovaris M, Pagani E, Sormani MP, Comi G, Filippi M. Magnetization transfer MRI metrics predict the accumulation of disability 8 years later in patients with multiple sclerosis. Brain 2006; 129(Pt 10):2620–2627.
121. Pitt D, Boster A, Pei W, et al. Imaging cortical lesions in multiple sclerosis with ultra-high-field magnetic resonance imaging. Arch Neurol 2010; 67:812–818.
122. Bonnier G, Roche A, Romascano D, et al. Advanced MRI unravels the nature of tissue alterations in early multiple sclerosis. Ann Clin Transl Neurol 2014; 1:423–432.
123. Bell JE. An update on the neuropathology of HIV in the HAART era. Histopathology 2004; 45:549–559.
124. Wu Y, Storey P, Carrillo A, et al. Whole brain and localized magnetization transfer measurements are associated with cognitive impairment in patients infected with human immunodeficiency virus. AJNR Am J Neuroradiol 2008; 29:140–145.
125. Granziera C, Daducci A, Simioni S, et al. Microstructural brain alterations in aviremic HIV+ patients with minor neurocognitive disorders: a multi-contrast study at high field. PLoS One. 2013; 8: e72547. doi: 10.1371/journal.pone.0072547.eCollection 2013.
126. Kurki T, Lundbom N, Kalimo H, Valtonen S. MR classification of brain gliomas: value of magnetization transfer and conventional imaging. Magn Reson Imaging 1995; 13:501–511.
127. Kurki T, Lundbom N, Komu M, Kormano M. Tissue characterization of intracranial tumors by magnetization transfer and spin-lattice relaxation parameters *in vivo*. J Magn Reson Imaging 1996; 6: 573–579.
128. Lundbom N. Determination of magnetization transfer contrast in tissue: an MR imaging study of brain tumors. AJR Am J Roentgenol 1992; 159:1279–1285.
129. Boorstein JM, Wong KT, Grossman RI, Bolinger L, McGowan JC. Metastatic lesions of the brain: imaging with magnetization transfer. Radiology 1994; 191:799–803.